Supplementary data for article :

Todorović, T. R.; Vukašinović, J.; Portalone, G.; Suleiman, S.; Gligorijević, N.; Bjelogrlić, S.; Jovanović, K.; Radulović, S.; Anđelković, K.; Cassar, A.; et al. (Chalcogen)Semicarbazones and Their Cobalt Complexes Differentiate HL-60 Myeloid Leukaemia Cells and Are Cytotoxic towards Tumor Cell Lines. *MedChemComm* **2017**, *8* (1), 103–111. https://doi.org/10.1039/c6md00501b

ELECTRONIC SUPPLEMENTARY INFORMATION

(Chalcogen)semicarbazones and their cobalt complexes differentiate HL-60 myeloid leukaemia cells and are cytotoxic towards tumor cell lines

Tamara R. Todorović[a], Jelena Vukašinović[a], Gustavo Portalone[b], Sherif Suleiman[c], Nevenka Gligorijević[d], Snezana Bjelogrlić[d], Katarina Jovanović[d], Siniša Radulović[d], Katarina Anđelković[a], Analisse Cassar[c], Nenad R. Filipović[e*], Pierre Schembri-Wismayer[c*]

[a]*Faculty of Chemistry, University of Belgrade, Studentski trg 12-16, 11000 Belgrade, Serbia;*

[b]*Department of Chemistry, Sapienza University of Rome, P.le Aldo Moro 5, 00185 Rome, Italy;*

[c]*Anatomy Department, Faculty of Medicine and Surgery, University of Malta, Malta; E-mail: pierre.schembri-wismayer@um.edu.mt*

[d]*Institute for Oncology and Radiology of Serbia, Pasterova 14, 11000 Belgrade, Serbia;*

[e]*Faculty of Agriculture, University of Belgrade, Nemanjina 6, 11081 Belgrade, Serbia; E-mail: nenadf.chem@gmail.com*

Corresponding authors:

Nenad R. Filipović, E-mail: nenadf.chem@gmail.com

Pierre Schembri-Wismayer, E-mail: pierre.schembri-wismayer@um.edu.mt

Electronic Supplementary Information Content:

EXPERIMENTAL PART

Materials and methods

Semicarbazide hydrochloride (99+%), thiosemicarbazide (98+%) and selenosemicarbazide (98%) were obtained from Acros Organics (BVBA, Geel, Belgium). 8-Quinolinecarboxaldehyde was obtained from MAYBRIDGE (England), while cobalt(II) perchlorate hexahydrate and cobalt(II) chloride hexahydrate were obtained from Aldrich (Sigma-Aldrich Chemie GmbH, Steinheim, Germany). All solvents (reagent grade) were obtained from commercial suppliers and used without further purification.

Elemental analyses (C, H, N, S) were performed by standard micromethods using the ELEMENTARVario ELIII C.H.N.S=O analyzer. IR spectra were recorded on a Thermo Scientific Nicolet 6700 FT-IR spectrophotometer by the Attenuated Total Reflection (ATR) technique in the region 4000–400 cm^{-1}. Molar conductivity measurements were performed at ambient temperature (298 K) on the Crison Multimeter MM41. ^{1}H NMR spectrum of H8qaSC ligand was recorded on Varian Gemini 2000 spectrometer. All other NMR spectra were performed on Bruker Avance 500 equipped with broad-band direct probe. Chemical shifts are given on δ scale relative to tetramethylsilane (TMS) as internal standard for ^{1}H and ^{13}C. UV-Visible (UV-Vis) spectra were recorded on a GBC Scientific Eq. PTY LTD Cintra 6 UV-Vis spectrophotometer, using samples dissolved in methanol (900–220 nm). For stability measurements the samples were dissolved in DMSO and diluted with water such that the final DMSO content was 1 vol.%. The magnetic measurement at room temperature was performed by Evans' method using a MSB-MK1 balance (Sherwood Scientific Ltd.) with $Hg[Co(SCN)_4]$ as a calibrant. Diamagnetic corrections were calculated from Pascal's constants.

Synthesis of ligands H8qaSC, H8qaTSC and H8qaSeSC

The ligands H8qaSC, H8qaTSC and H8qaSeSC were synthesized according to the reported procedures [S1-S3]. The chemical structures of the compounds were confirmed by elemental analysis, IR and NMR spectroscopy. The ligands were recrystallized by slow diffusion of ethanol into the DMSO solution of the corresponding ligand. In the case of ligand H8qaTSC, single crystals suitable for X-ray analysis were obtained.

Synthesis of the complexes $[Co(H8qaSC)_2]Cl_2{\cdot}2H_2O$ (1), $[Co(8qaTSC)_2]ClO_4{\cdot}DMSO$ (2) and $[Co(8qaSeSC)_2]ClO_4{\cdot}DMSO$ (3)

Cobalt complexes with H8qaSC and H8qaTSC ligands were prepared according to a general procedure: into the suspension of 8-quinolinecarboxaldehyde (0.10 g, 0.63 mmol) and semicarbazide hydrochloride (0.07 g, 0.63 mmol) or thiosemicarbazide (0.06 g, 0.66 mmol) in ethanol (10 mL) the corresponding metal salt was added [$CoCl_2{\times}6H_2O$: 0.09 g, 0.32 mmol in the case of complex **1** or $Co(ClO_4)_2{\times}6H_2O$: 0.12 g, 0.32 mmol in the case of complex **2**]. The

reaction mixture was stirred under the reflux for 2 h. Cobalt complex **3** with the ligand H8qaSeSC was synthesized according to the reported procedure [S4].

(**1**): Light-orange single crystals, obtained from the mother liquor, were filtered off, washed with cold ethanol and diethyl ether, and dried *in vacuo*. Yield: 0.12 g (46.7%). Anal. Calcd. for $C_{22}H_{24}N_8Cl_2O_4Co$ (MW = 594.31): C, 44.46; H, 4.07; N, 18.85. Found: C, 44.89; H, 3.91; N, 18.78 %. IR (ATR, cm^{-1}): 3392, 3293, 3151, 3058, 3000, 2940, 2839, 2724, 2166, 1652, 1623, 1599, 1579, 1551, 1506, 1433, 1395, 1366, 1259, 1180, 1144, 1088, 1022, 973, 912, 833, 789, 764, 745, 671, 584, 533, 512, 490, 445, 419. Λ_M ($1 \cdot 10^{-3}$ M, ethanol): 127.3 Ω^{-1} cm^2 mol^{-1}. UV-Vis (MeOH), λ_{max}, nm (ε, M^{-1} cm^{-1}): 237 (40482), 263 shoulder (sh) (20556), 321 (24395), 398sh (2152). μ(298 K) = 1.80 μB.

(**2**): Brown microcrystalline product was filtered off and washed with cold ethanol and diethyl ether. Dark brown single crystals of **2** were obtained by slow diffusion of ethanol into the DMSO solution of the complex. Yield: 0.16 g (58%). IR (ATR, cm^{-1}): 3384, 3289, 3117, 2798, 1637, 1578, 1500, 1429, 1394, 1336, 1302, 1262, 1186, 1160, 1091, 1015, 940, 916, 834, 768, 718, 620, 542, 498, 453, 423, 405. ^{1}H NMR (500 MHz, DMSO-d_6) δ (ppm): 2.54 (s, 3H, DMSO), 7.13 (s, 2H, H–N4), 7.60 (dd, 1H, H–C3, ^3J = 8.1 Hz, ^3J = 5.4 Hz), 7.98 (t, 1H, H–C6, $^3J_{6,5}$ = $^3J_{6.7}$ = 7.8 Hz), 8.33 (dd, 1H, H–C5, $^3J_{5,6}$ = 7.8 Hz, $^4J_{5,7}$ = 1.1 Hz), 8.49 (dd, 1H, H–C7, $^3J_{7,6}$ = 7.8 Hz, $^4J_{7,5}$ = 1.1 Hz), 8.68-8.72 (m, 2H, H–C4 and H–C2), 9.03 (s, 1H, H–C9). ^{13}C NMR (126 MHz, DMSO-d_6) δ (ppm): 40.42 (DMSO), 123.22 (C3), 128.03 (C6), 128.47 (C8), 130.13 (C4a), 133.92 (C5), 138.32 (C8a), 138.63 (C7), 141.10 (C4), 152.30 (C9), 155.43 (C2), 176.14 (C10). Λ_M ($1 \cdot 10^{-3}$ M, DMSO): 34.9 Ω^{-1} cm^2 mol^{-1}. UV-Vis (MeOH), λ_{max}, nm (ε, M^{-1} cm^{-1}): 247 (34887), 309 (22588), 338 (18811), 406 broad (12535). Magnetic measurements showed that obtained complex is diamagnetic.

Direct syntheses of the novel complexes starting from appropriate metal salts and the ligands in ethanol afforded identical products as the template syntheses, but with a slightly lower yield.

X-ray crystallography

The intensity data were collected on the Oxford Diffraction Xcalibur S CCD diffractometer with graphite-monochromated Mo Kα radiation (λ = 0.710689 Å) at 298(2) K operated at 50 kV and 40 mA. The data reductions were performed using the CrysAlis software package [S5]. Solution, refinement and analysis of the structures were performed using the programs integrated in the WinGX system [S6]. The crystal structures were solved by direct methods using SIR2002 [S7] and refined by the full-matrix least-squares method based on F^2 using SHELXL-2014/7 [S8]. All non-hydrogen atoms were refined anisotropically until convergence was reached. The hydrogen atoms were located in a difference Fourier map and refined isotropically, with the exception of those H atoms linked to the C atoms and those H atoms linked to the N atoms (in **2**) which were placed in calculated positions (C–H = 0.97 Å,

N–H = 0.86 Å, U_{iso} values equal to 1.2 U_{eq} C, N) and allowed to ride on their carrier atoms. In **2**, the sulfur atom from the DMSO molecule is disordered over two sites with occupation factors 0.85 and 0.15 and therefore the hydrogen atoms of crystalline solvent were not positioned and refined. Geometrical calculations were performed using PLATON [S9]. Crystallographic data for the structures reported in this paper have been deposited with the Cambridge Crystallographic Data Center as supplementary publication nos. CCDC 1401684–1401686. Copies of the data can be obtained free of charge on application to The Director, CCDC, 12 Union Road, Cambridge CB2 1EZ, UK (fax: +44 1223 336 033; e-mail: deposit@ccdc.cam.ac.uk).

Cell culture

HL-60 (myeloid leukaemia) cells (ATCC® CCL-240™) were maintained in Rose Park Memorial Institute (RPMI) 1640 medium (Sigma-Aldrich, R6504) prepared with 2 g/L sodium bicarbonate, and supplemented with 10 % fetal bovine serum (Sigma-Aldrich, F4135), penicillin (100 units/mL), and streptomycin (100 µg/mL). Cells were kept at 37 °C in atmosphere containing 5% CO_2 with twice weekly subculturing.

Human cervix carcinoma cells (HeLa), lung adenocarcinoma cells (A549), human colon cancer cells (LS-174), breast cancer cells (MDA-MB-361) and human fetal lung fibroblast cells (MRC-5) were maintained as monolayer culture in the Roswell Park Memorial Institute (RPMI) 1640 nutrient medium (Sigma Chemicals Co, USA). Human myelogenous leukemia cells (K562) were maintained in suspension culture. RPMI 1640 was prepared in sterile deionized water, supplemented with penicillin (192 IU/mL), streptomycin (200 µg/mL), 4-(2-hydroxyethyl)piperazine-1-ethanesulfonic acid (HEPES) (25 mM), L-glutamine (3 mM) and 10% heat-inactivated fetal calf serum (FCS) (pH 7.2). The cells were grown at 37 ºC in a 5% (v/v) CO_2 humidified air atmosphere, with twice weekly subculturing.

Differentiation Induction

HL-60 cells were seeded in 96 well tissue culture plates at density of 5000 per well for 3 day treatment and 3000 per well for 5 day treatment due to differences in proliferation. All investigated compounds were initially dissolved in DMSO to stock concentrations of 10 mM, whereas further dilutions were performed with the RPMI 1640 medium immediately before each experiment. All tested compounds were added in a range of five concentrations (up to 30 µM). Phorbol myristate acetate (PMA) at concentrations of 10 and 100 nM, were also tested in triplicates as positive controls for granulocytic and monocytic differentiation, respectively. The negative control for each set was a well containing only RPMI medium without any added inducers. At the end of incubation period (of 3 or 5 days), plates were placed on a shaker for 5 min and afterwards, the contents of each well (200 µL) were split in half with half being transferred to another 96 well plate. One of the plates was tested with the 3-(4,5-

dimethylthiazol-2yl)-2,5-diphenyltetrazolium bromide (MTT, Sigma) assay and the other by the Nitroblue tetrazolium (NBT, Sigma-Aldrich, N6876) assay.

Differentiation screening assay

A modification of the quantitative protocol was used [S10]. Briefly, NBT was dissolved in water at a concentration of 2 mg/mL on the day of testing (solution made afresh). The 96 well plates containing the HL-60 cells were centrifuged at 800*g* for 10 min. After removing the supernatant, 200 µL activated NBT, with addition of PMA to a final concentration of 1 µg/mL just before testing, were placed in each well and incubated for 25 min. After this, 70 µL 1 M HCl was used to stop the reaction. The plates were once again centrifuged at 800*g* for 10 min. After removing the supernatant, 50 µL 2 M KOH and 150 µL DMSO were added. The plates were then transferred to the spectrophotometer (SPECTROstar Nano, BMG Labtech GmbH, Ostenberg, Germany) where absorbance was recorded at a wavelength of 630 nm with a 405 nm reference wavelength.

To assess relative cell number, 20 µL of 5 mg/mL of MTT dissolved in phosphate buffer saline solution (PBS) was added in each well being tested and incubated at 37 °C for 4 h. The plate was then centrifuged at 800*g* for 10 min and supernatant was removed. Formazan crystals produced were dissolved by addition of 120 µL DMSO and absorbance was read on a spectrophotometer (SPECTROstar Nano, BMG Labtech GmbH, Ostenberg, Germany) at 570 nm, with a reference wavelength at 690 nm. Undifferentiated cells continue to proliferate, whilst those which entered differentiation will be reduced in number as more mature forms of myeloid cells stop proliferating as part of their maturation process. They also become capable of NBT reduction. Therefore, the NBT/MTT ratio is used as a screening method to gauge differentiation induction in this model cell line.

Cell morphology assessment

For morphological analysis, cells were seeded in 96 well plates for a 3 day and a 5 day incubation at the same concentration as tested above. At the end of the incubation period, the well contents were harvested and transferred onto glass slides using a cytocentrifuge (Shandon CytoSpin II, GMI, Minnesota, USA). After the slides were air dried for at least 5 min, freshly prepared Leishman's stain (AppliChem, A4277) in methanol at a concentration of 1.5 g/L of was applied to fully cover the slides. After 2 min, twice the amount of PBS was added and mixed by swirling. Slides were left for another 15 min to incubate, rinsed thoroughly with distilled water and left to dry for visualization. Triplicate slides were scored for signs of differentiation, which

were then tabulated. The slides were viewed microscopically (Motic AE2000 microscope with Moticam PRO 282A digital camera).

MTT assay

Cytotoxicity of the investigated ligands, their cobalt complexes and reference compound cisplatin (CDDP), was determined using MTT assay [S11]. Cells were seeded in 96-well cell culture plates (Thermo Scientific) HeLa (4000 cells/well), A549 (8000 cells/well), LS-174 (7000 cells/well), MDA-MB-361 (7000 cells/well) and MRC-5 (6000 cells/well) in culture medium and grown for 24 h. Stock solutions of investigated complexes and ligands were made in DMSO at a concentration of 10 mM, and afterwards diluted with nutrient medium to the desired final concentrations (in the range up to 100 μM). CDDP stock solution was made in 0.9% NaCl at a concentration of 1.66 mM and afterwards diluted with nutrient medium to the desired final concentrations (in the range up to 100 μM). The final concentration of DMSO in wells with investigated compounds was less than 1% (v/v). Solutions of the various concentrations of the examined compounds were added to the wells, except for the control wells where only nutrient medium was added. All samples were tested in triplicate. Nutrient medium with corresponding agent concentrations but without target cells was used as a blank, also in triplicate. Cells were incubated for 48 h with the test compounds at 37 ºC, with 5% (v/v) CO_2 in a humidified atmosphere. After incubation, the MTT assay was performed, as previously described [S12]. Absorbance was recorded on the ThermoLabsystems 408 Multiskan EX 200–240 V at a wavelength of 570 nm. Concentration IC_{50} (μM) was defined as the concentration of a substance producing 50% inhibition of cell survival. It is determined from the cell survival curves.

Cell cycle analysis

The effect of the ligands and complexes **1**–**3** on the cell cycle phase distribution was performed by flow cytometry. DNA content in fixed HeLa cells and A549 cells (only complex **1**), were analyzed after staining with propidium iodide (PI) [S13]. Cells were seeded at density of 2×10^5 cells/well in a 6-well plate (Thermo Scientific) and grown in nutrient medium. After 24 h, cells were continually exposed to the tested substances with concentrations that correspond to IC_{50} and $1.5 \times IC_{50}$ (determined for 48 h treatment). Control cells were incubated only in nutrient medium. After 24 and 48 h of continual exposure to the substances, cells were analyzed as previously described [S14]. Cell cycle phase distributions were analyzed using a FASC Calibur Becton Dickinson flow cytometer and Cell Quest Pro computer software.

Fluorescent microscopy

Morphological characteristics of HeLa cell death induced by the treatment with investigated substances were analyzed after staining of the treated cells with a mixture of acridine orange (AO) and ethidium bromide (EB) [S15]. Briefly, 1×10^5 of HeLa cells were

seeded on a glass slide in Petri dishes, and after 24 h exposed to IC_{50} concentrations of investigated compounds for the next 24 and 48 h. The cells were then stained with 10 μL of a mixture of a working concentration of AO/EB: 3 μg/mL AO and 10 μg/mL EB in phosphate-buffered saline (PBS) solution, and observed for the next 30 min under a fluorescence microscope Axio Observer Z1, using AxioVision imaging software (Carl Zeiss MicroImaging GmbH).

Apoptotic assay

Induction of apoptosis by the ligands, complexes **1**–**3** and CDDP in HeLa cells was determined by Annexin-V–FITC (fluorescein isothiocyanate) apoptosis detection kit, according to the manufacturer's instructions (BD Biosciences). Briefly, suspended HeLa cells (1×10^6 cells/mL) were exposed to IC_{50} concentrations of investigated compounds for 24 and 48 h. Afterwards, cells were tyrpsinized, washed twice with cold PBS and then re-suspended in 200 μL binding buffer (10 mM HEPES/NaOH, pH 7.4, 140 mM NaCl, 2.5 mM $CaCl_2$). A volume of 100 μL of the solution (1×10^5 cells) was transferred to a 5 mL culture tube and 5 μL of Annexin-V–FITC and 5 μL of PI were than added. Cells were gently vortexed and incubated for 15 min at 25 °C in the dark. A volume of 400 μL binding buffer was then added to each tube and the cells analyzed using a FACS Calibur Becton Dickinson flow cytometer and Cell Quest Pro computer software.

RESULTS & DISCUSSION

Description of structures

Table S1. Bond lengths (Å) and angles (°) for the complexes 1 and 2, with esd's in parentheses.

1		**2**	
Co(1)–N(2) = Co(1)–N(2)^{ia}	2.0628(18)	Co(1)–N(2)	1.917(2)
Co(1)–O(1) = Co(1)–O(1)^{i}	2.0922(16)	Co(1)–N(2A)	1.914(2)
Co(1)–N(1) = Co(1)–N(1)^{i}	2.1279(19)	Co(1)–N(1A)	2.019(2)
N(2)–C(11) = N(2)i–C(11)^{i}	1.283(3)	Co(1)–N(1)	2.032(2)
N(2)–N(3) = N(2)^{i}–N(3)^{i}	1.371(3)	Co(1)–S(2)	2.2101(8)
N(3)–C(12) = N(3)^{i}–C(12)^{i}	1.360(3)	Co(1)–S(1)	2.2108(8)
N(4)–C(12) = N(4)^{i}–C(12)^{i}	1.325(3)	S(1)–C(12)	1.728(3)
O(1)–C(12) = O(1)^{i}–C(12)^{i}	1.246(3)	S(2)–C(12A)	1.730(3)
N(2)–Co(1)–N(2)^{i}	162.87(11)	N(2A)–Co(1)–N(2)	167.90(9)
O(1)–Co(1)–O(1)^{i}	92.17(10)	N(2A)–Co(1)–N(1A)	95.48(9)
N(1)–Co(1)–N(1)^{i}	91.41(11)	N(2)–Co(1)–N(1A)	93.85(9)
N(2)–Co(1)–O(1) = N(2)^{i}–Co(1)–O(1)^{i}	77.76(7)	N(2A)–Co(1)–N(1)	93.27(10)
N(2)^{i}–Co(1)–O(1) = N(2)–Co(1)–O(1)^{i}	90.32(7)	N(2)–Co(1)–N(1)	94.78(10)
N(2)–Co(1)–N(1) = N(2)^{i}–Co(1)–N(1)^{i}	103.70(7)	N(1A)–Co(1)–N(1)	87.80(10)
N(2)^{i}–Co(1)–N(1) = N(2)–Co(1)–N(1)^{i}	88.34(7)	N(2A)–Co(1)–S(1)	85.83(7)
O(1)–Co(1)–N(1) = O(1)^{i}–Co(1)–N(1)^{i}	89.92(7)	N(2)–Co(1)–S(2)	84.62(7)
O(1)^{i}–Co(1)–N(1) = O(1)–Co(1)–N(1)^{i}	165.95(6)	N(1A)–Co(1)–S(2)	177.79(7)
C(12)–O(1)–Co(1) = C(12)^{i}–O(1)^{i}–Co(1)	113.39(15)	N(1)–Co(1)–S(2)	90.74(7)
N(3)–N(2)–Co(1) = N(3)^{i}–N(2)^{i}–Co(1)	111.74(14)	N(2A)–Co(1)–S(2)	86.26(7)
C(10)–N(1)–Co(1) = C(10)^{i}–N(1)^{i}–Co(1)	127.83(14)	N(2)–Co(1)–S(1)	86.50(7)
C(11)–N(2)–Co(1) = C(11)^{i}–N(2)^{i}–Co(1)	129.47(16)	N(1A)–Co(1)–S(1)	89.88(7)
O(1)–C(12)–N(3) = O(1)^{i}–C(12)^{i}–N(3)^{i}	120.6(2)	N(1)–Co(1)–S(1)	177.42(7)
C(12)–N(3)–N(2) = C(12)^{i}–N(3)^{i}–N(2)^{i}	116.42(19)	S(2)–Co(1)–S(1)	91.62(3)

[a] Symmetry transformations used to generate equivalent atoms: $i = -x, y, 1.5 - z$.

Crystal packing in the crystal structures 1 and 2

Crystal packing of complex **1** is based on 3D hydrogen bond network (Figure S1). Each chloride ion is involved, as an acceptor, in hydrogen bonding with two water molecules and N3–H group, while oxygen atoms from water molecules are acceptors in interactions with $N4H_2$ group (Table S2).

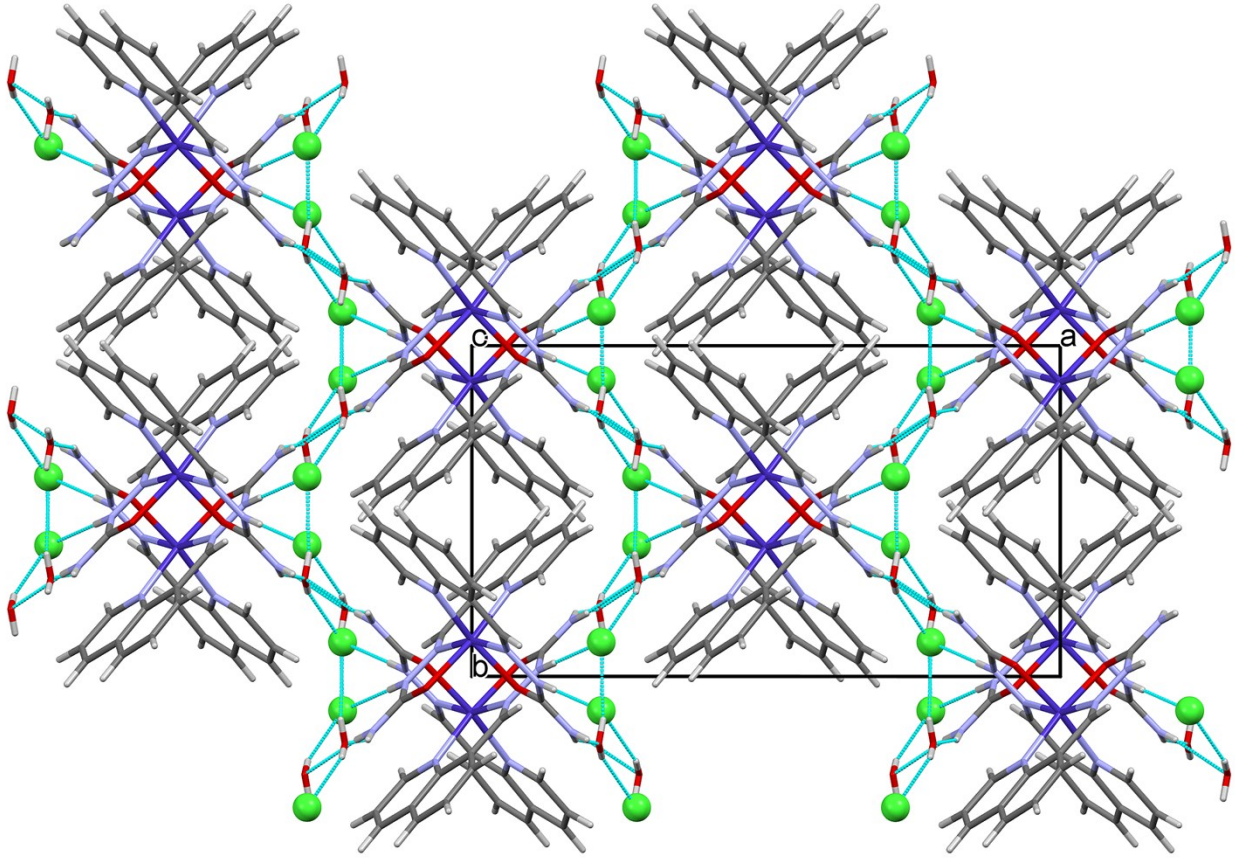

Figure S1. Crystal packing in the crystal structure of complex **1** viewed along the *c*-axis. Color code: chlorine – green, oxygen – red, cobalt - dark blue, nitrogen – light blue, carbon – grey, hydrogen – white.

Table S2. Hydrogen bond parameters in the crystal structure of complex **1**

D–H···A	D–H (Å)	H···A (Å)	D···A (Å)	D–H···A (°)	symmetry operation on A
O1W–H1W···Cl1	0.76	2.38(4)	3.125(3)	168(4)	
O1W–H2W···Cl1	0.78	2.35(3)	3.077(3)	155(4)	$1/2 - x, -1/2 + y, 5/2 - z$
N3–H···Cl1	0.83	2.32(4)	3.144(3)	177(3)	$x, -y, -1/2 + z$
N4–H4A···O1W	0.83	2.13(4)	2.934(3)	163(3)	
N4–H4B···O1W	0.81	2.19(4)	2.960(5)	159(2)	$1/2 - x, -1/2 - y, 2 - z$

In the crystal structure of the complex **2** 1-D infinite chains are formed due to hydrogen bonding between neighbouring complex cations (Figure S2A). Perchlorate anions and solvent DMSO molecules also participate in the hydrogen bonding. The stacking interactions between neighboring pyridine fragments expand 1-D chains formed by hydrogen bonding into 2-D supramolecular layers parallel to (001). Finally, these 2-D layers are further interlinked into a 3-D framework (Figure S2B) by additional stacking interactions. The geometrical parameters describing hydrogen bonding and π-π interactions in **2** are given in Table S2.

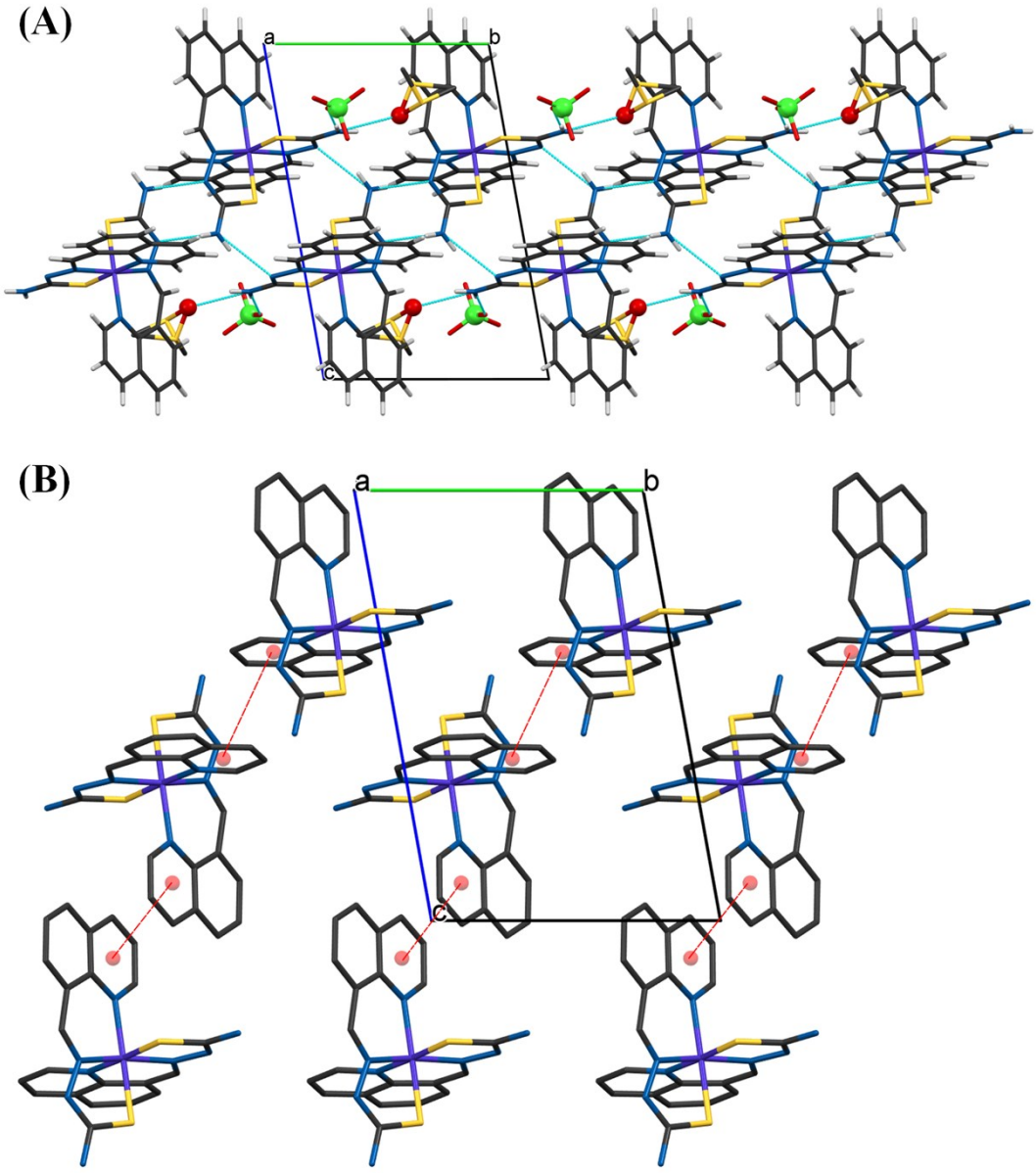

Figure S2. Crystal packing in the crystal structure of complex **2** viewed along the *a*-axis. Color code: chlorine – green, oxygen – red, cobalt - purple, nitrogen – blue, sulfur – yellow, carbon – grey, hydrogen – white. (A) Infinite 1D chains, formed by hydrogen bonding, parallel to the *b*-axis. (B) π-π stacking interactions of quinoline fragments (red dashed lines); perchlorate anions, DMSO solvent molecules and hydrogen atoms are omitted for clarity.

Table S3. Hydrogen bond and π-π stacking interaction parameters in the crystal structure of complex **2**.

H-bond parameters					
D–H···A	D–H (Å)	H···A (Å)	D···A (Å)	D–H···A (°)	symmetry operation on A
complex **2**					
N4A–H4A1···O1	0.86	2.08	2.905(4)	159	
N4A–H4A2···O4	0.86	2.13	2.984(8)	171	
N4–H41···N3	0.86	2.14	2.991(4)	169	$2-x, 1-y, 1-z$
N4–H42···N3A	0.86	2.24	3.062(4)	160	$2-x, -y, 1-z$
π-π interaction parameters					
Cg(I),Cg(J)[a] Cg–Cg[b] (Å)	α[c] (°)	β[d] (°)	γ[e] (°)	slippage[f] (Å)	symmetry operation on J
complex **2**					
Cg1, Cg1 4.060(2)	0.01(1)	31.1	31.1	2.098	$2-x, -y, 2-z$
Cg2, Cg2 3.9305(1)	0.01(1)	30.4	30.4	1.991	$1-x, 1-y, 1-z$

[a] Planes of the rings I/J: ring (1) = N(1),C(2),C(3),C(4),C(5),C(10); ring (2) = N(1A),C(2A),C(3A),C(4A),C(5A),C(10A)
[b] Cg–Cg = distance between ring centroids (Å).
[c] α = dihedral angle between planes I and J (°).
[d] β = angle between Cg(I),Cg(J) vector and normal to plane I (°).
[e] γ = angle between Cg(I), Cg(J) vector and normal to plane J (°).
[f] Slippage = distance between Cg(I) and perpendicular projection of Cg(J) on ring I (Å).

Spectroscopic characterization

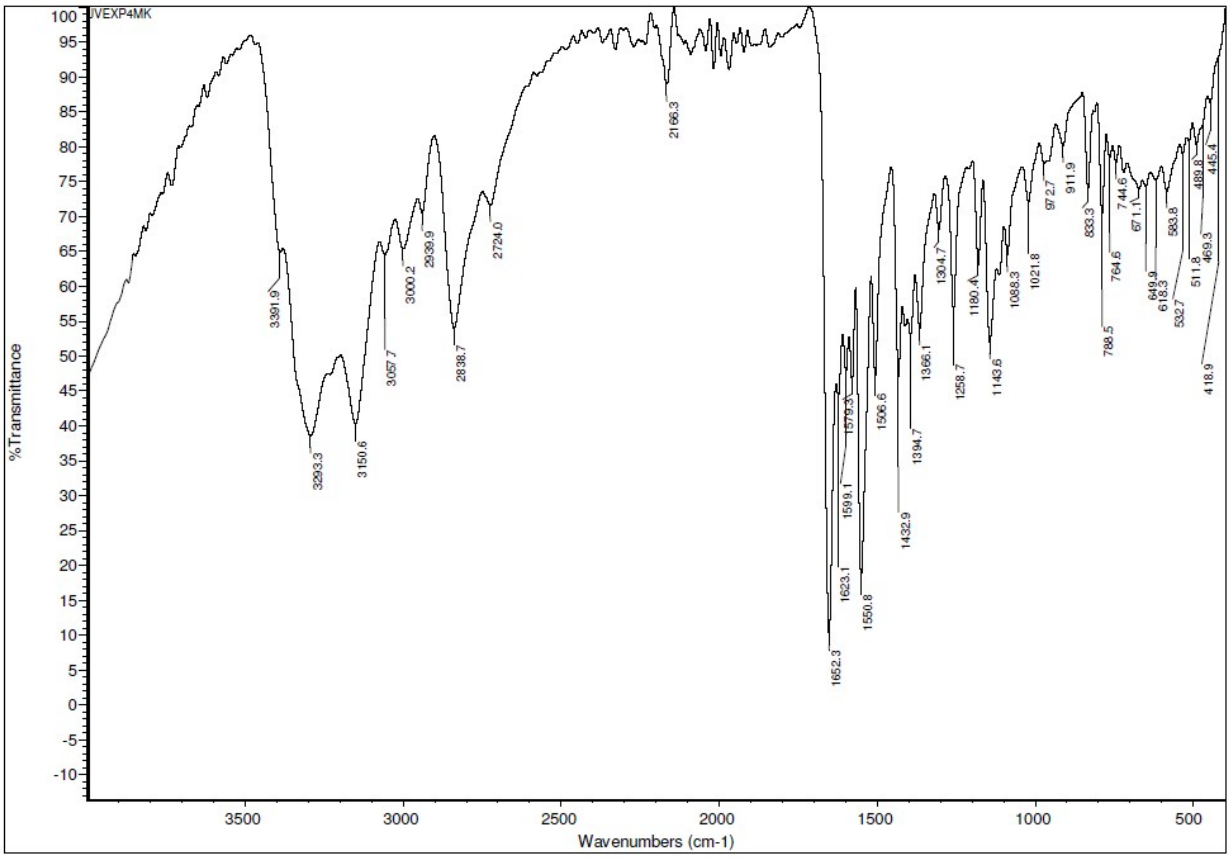

Figure S3. IR spectrum of the complex **1**

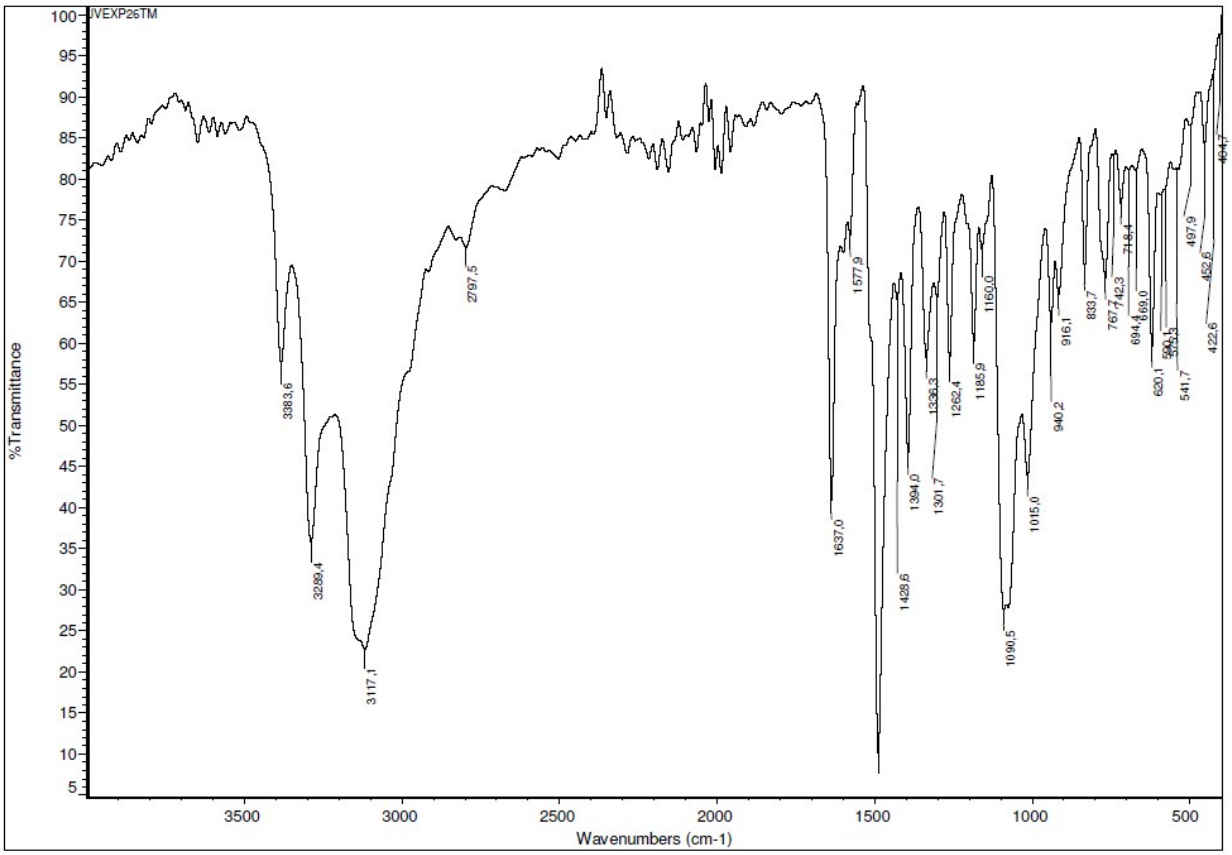

Figure S4. IR spectrum of the complex **2**

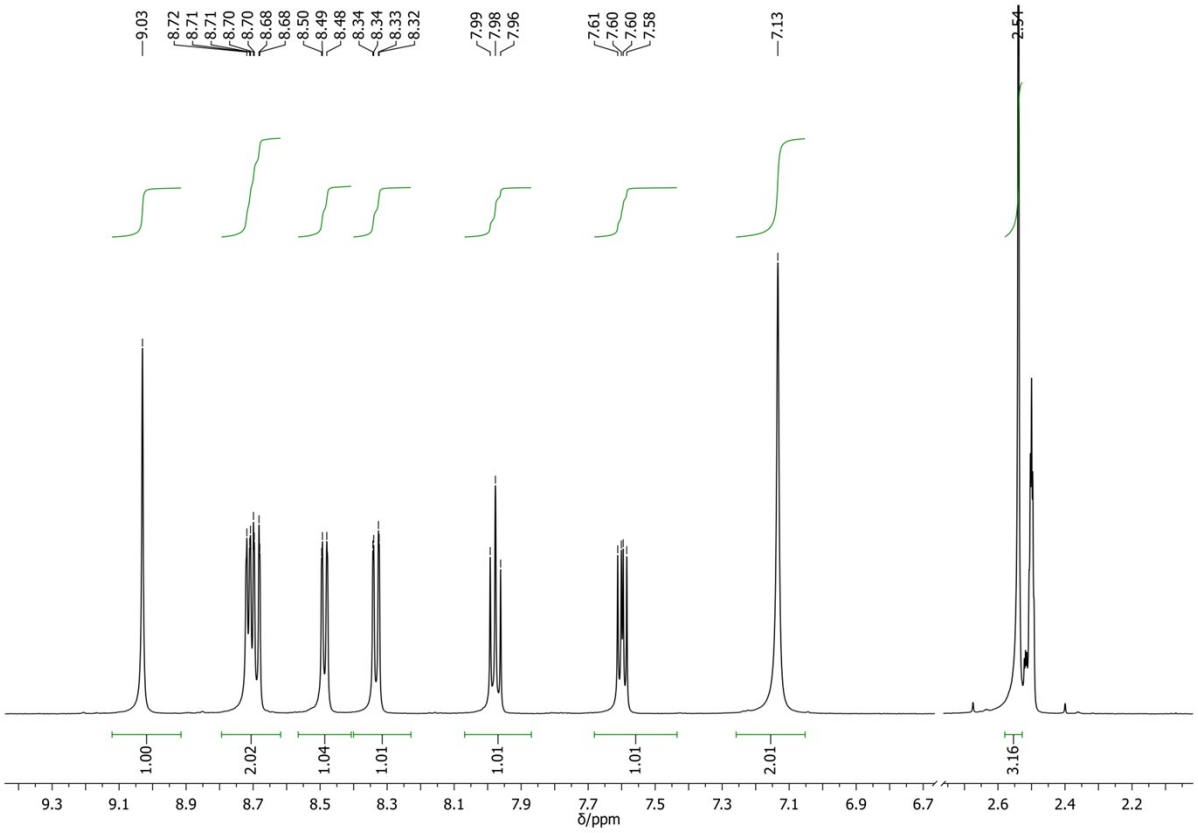

Figure S5. ^{1}H NMR spectrum of the complex **2**

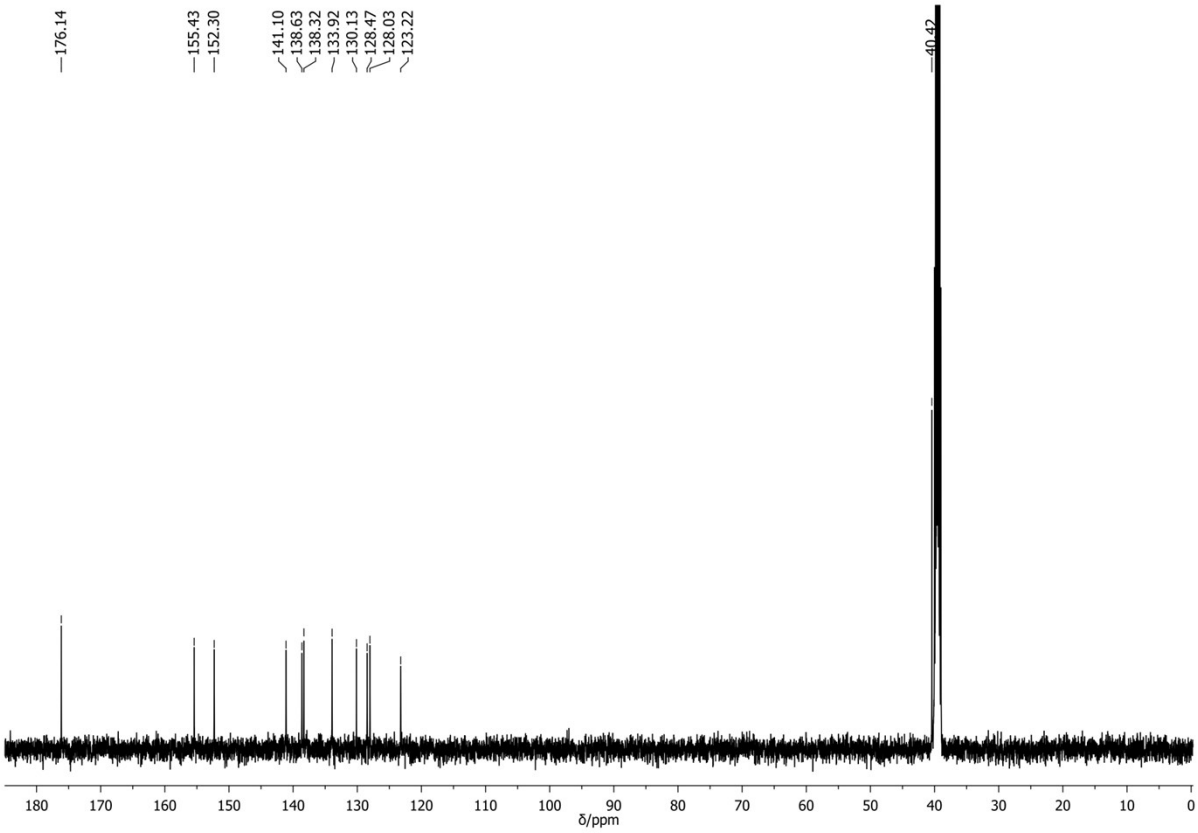

Figure S6. ^{13}C NMR spectrum of the complex **2**

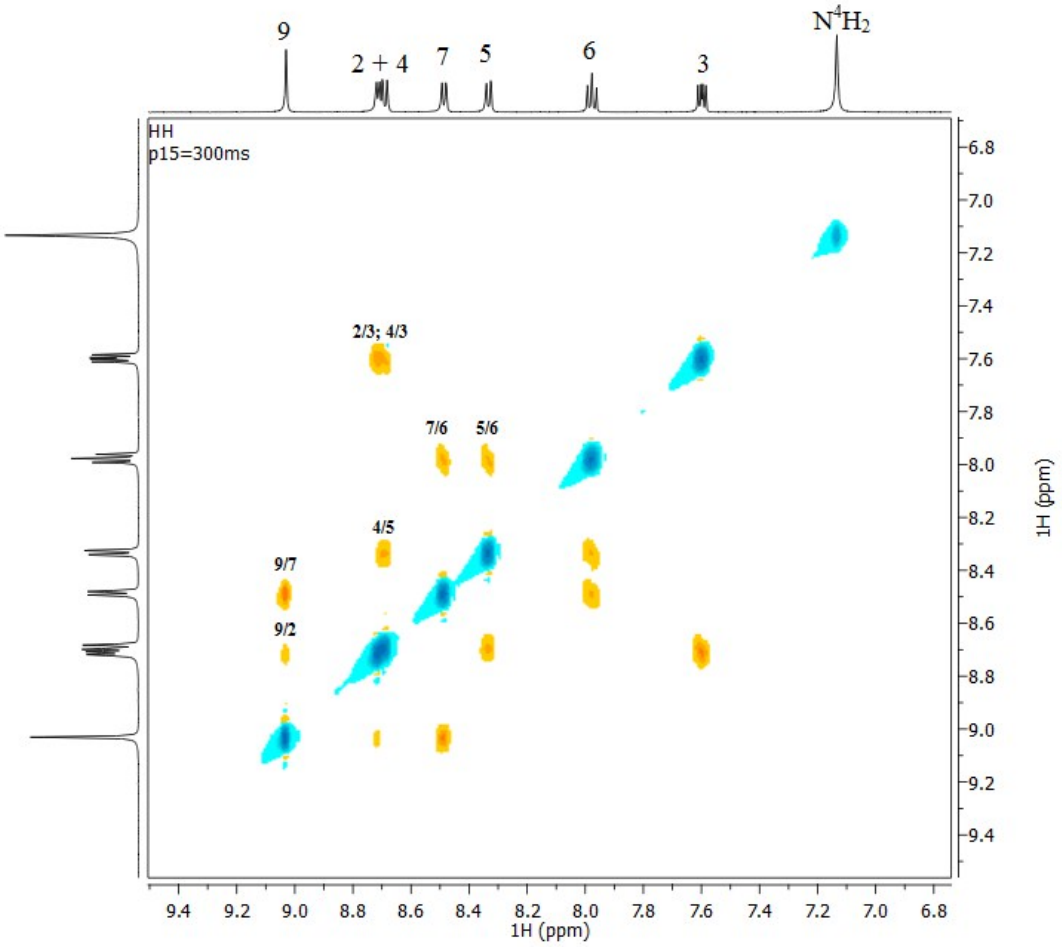

Figure S7. ROESY spectrum of the complex **2.**

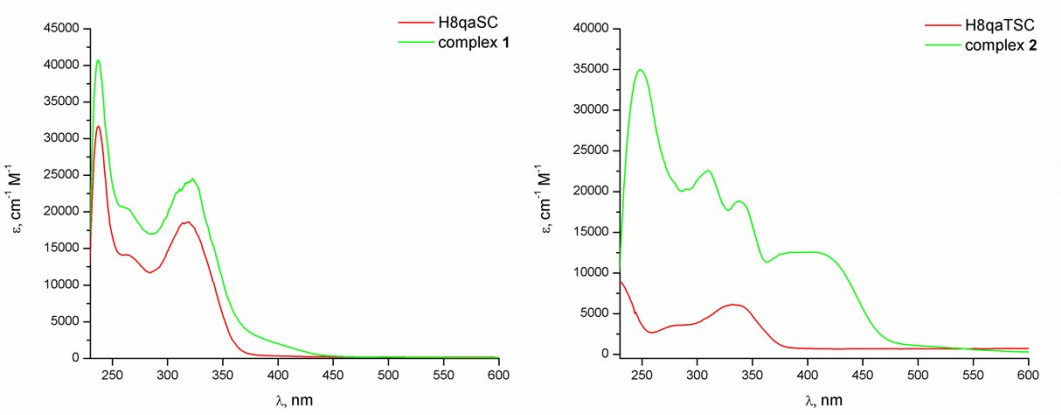

Figure S8. The electronic absorption spectra of the ligand H8qaSC and complex **1** (c = 5 × 10^{-5} M, left panel) and ligand H8qaTSC and complex **2** (c = 1 × 10^{-4} M, rignt panel) in methanol.

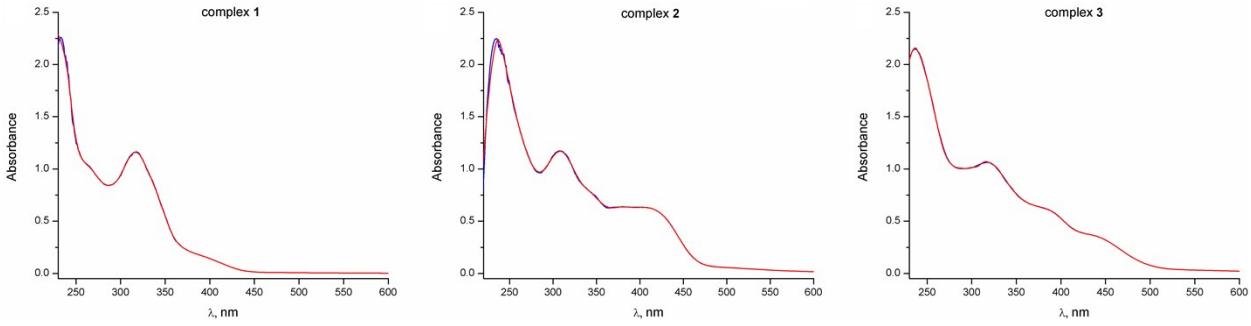

Figure S9. UV-Vis spectroscopy data of **1** (left panel), 2 (middle panel) and **3** (right panel) in DMSO/H_2O 1 : 100 (v/v). First measurement (red), after 24 h (blue).

Spectrophotometric assays of HL-60 differentiation-inducing and cytotoxic activity

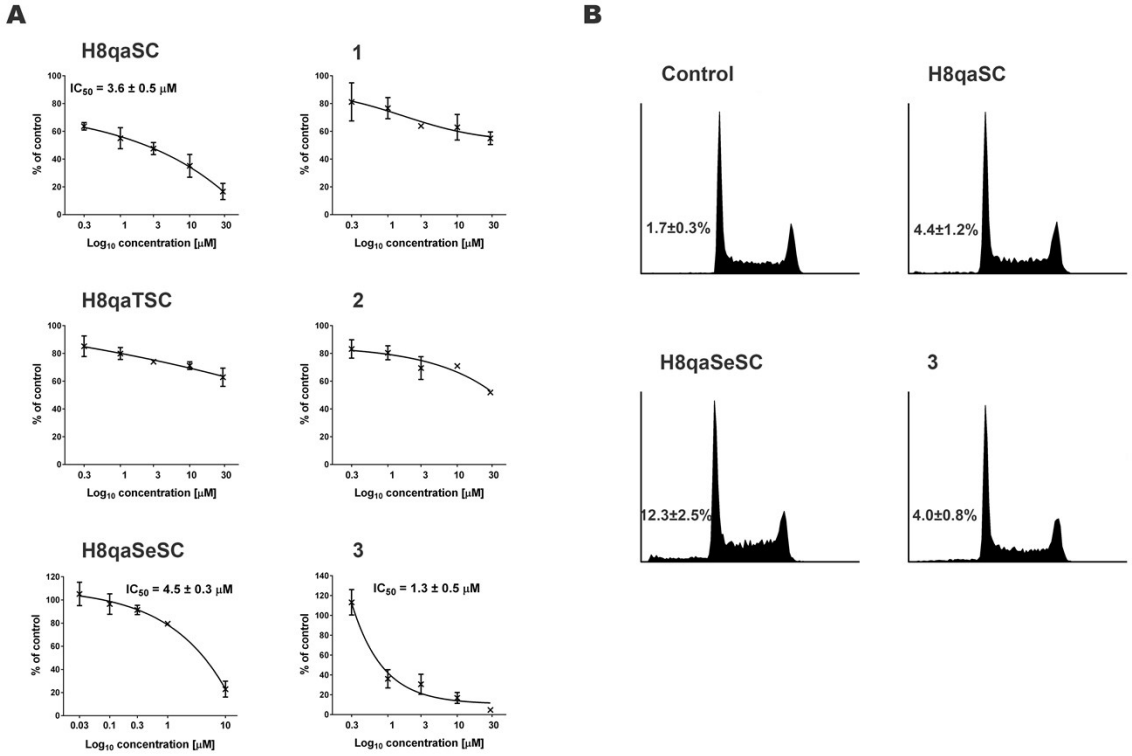

Figure S10. Concentration-response curves for investigated compounds applied in a range of five concentrations on HL60 cells after 72 h incubation (A). Cell cycle changes with sub-G1 fraction after 72 h treatment of investigated compounds applied in IC_{50} concentrations (B). All experiments have been performed in three replicates, with values expressed as the mean ± SD.

Differentiation results – morphology

Table S4. Feature scoring to indicate signs of differentiation. Slides prepared with 200 µL of cell suspension were spun down using cytocentrifugation and were reviewed by three separate reviewers with experience of haematological cytology. Despite the lack of a clear phenotype of a particular stage of normal differentiation, features indicate a clear trend. The values shown are mean percentage scores from three high power fields for each slide, reviewed by three investigators.

Differentiation-related features % per High Power Field (HPF)	Metaphases / HPF	Cells with nucleoli / HPF	Cells with euchromatin nuclei / HPF	Cells with lobed nuclei / HPF	Cells with irregular cytoplasm / HPF	Clearly granular cells / HPF	Cells with obvious vacuoles / HPF	Giant (fused) multinuclear cells	Apoptotic cells / HPF
Medium	1.8 ± 0.3	94.2 ± 2.2	97.1 ± 1.6	0.9 ± 0.4	35.3 ± 13.3	0.5 ± 0.9	0.2 ± 0.2	0.7 ± 0.6	0.8 ± 0.1
DMSO	0.00	0.00	0.8 ± 1.4	56.3 ±1.5	99.2 ± 1.5	7.0 ± 4.3	0.00	0.9 ± 1.5	11.5 ± 4.6
PMA	0.00	14.9 ± 0.4	1.7 ± 3.0	34.7 ± 1.0	54.5 ± 2.8	0.00	3.3 ± 1.6	2.5 ± 0.1	17.4 ± 0.5
H8qaSC	1.6 ± 1.5	1.0 ± 1.8	3.1 ± 5.4	29.7 ± 30.2	82.5 ± 7.1	3.6 ± 6.3	5.2 ± 5.6	1.0 ± 1.8	11.7 ± 2.7
H8qaTSC	1.0 ± 0.5	49.3 ± 40.8	53.9 ± 45.7	0.6 ± 0.8	5.7 ± 3.7	0.5 ± 0.3	0.2 ± 0.2	0.2 ± 0.1	0.5 ± 0.2
H8qaSeSC	1.7 ± 0.1	6.4 ± 4.0	101.8 ± 9.8	0.5 ± 0.3	5.9 ± 9.5	49.9 ± 12.8	0.2 ± 0.2	0.00	2.3 ± 1.8
1	6.7 ± 8.2	74.7 ± 3.8	89.2 ± 6.8	2.8 ± 2.3	21.1 ± 5.3	0.6 ± 0.3	2.4 ± 1.0	0.3 ± 0.2	3.2 ± 2.8
2	1.6 ± 0.2	73.0 ± 16.3	96.5 ± 2.8	0.6 ± 0.2	4.1 ± 1.4	0.9 ± 1.2	0.2 ± 0.2	0.1 ± 0.1	2.4 ± 1.2
3	1.5 ± 0.4	55.7 ± 20.0	95.4 ± 3.6	4.7 ± 3.0	72.1 ± 30.0	0.00	0.00	0.5 ± 0.6	3.1 ± 20.9

Cytotoxic effects on tumour cell lines and non-transformed cells

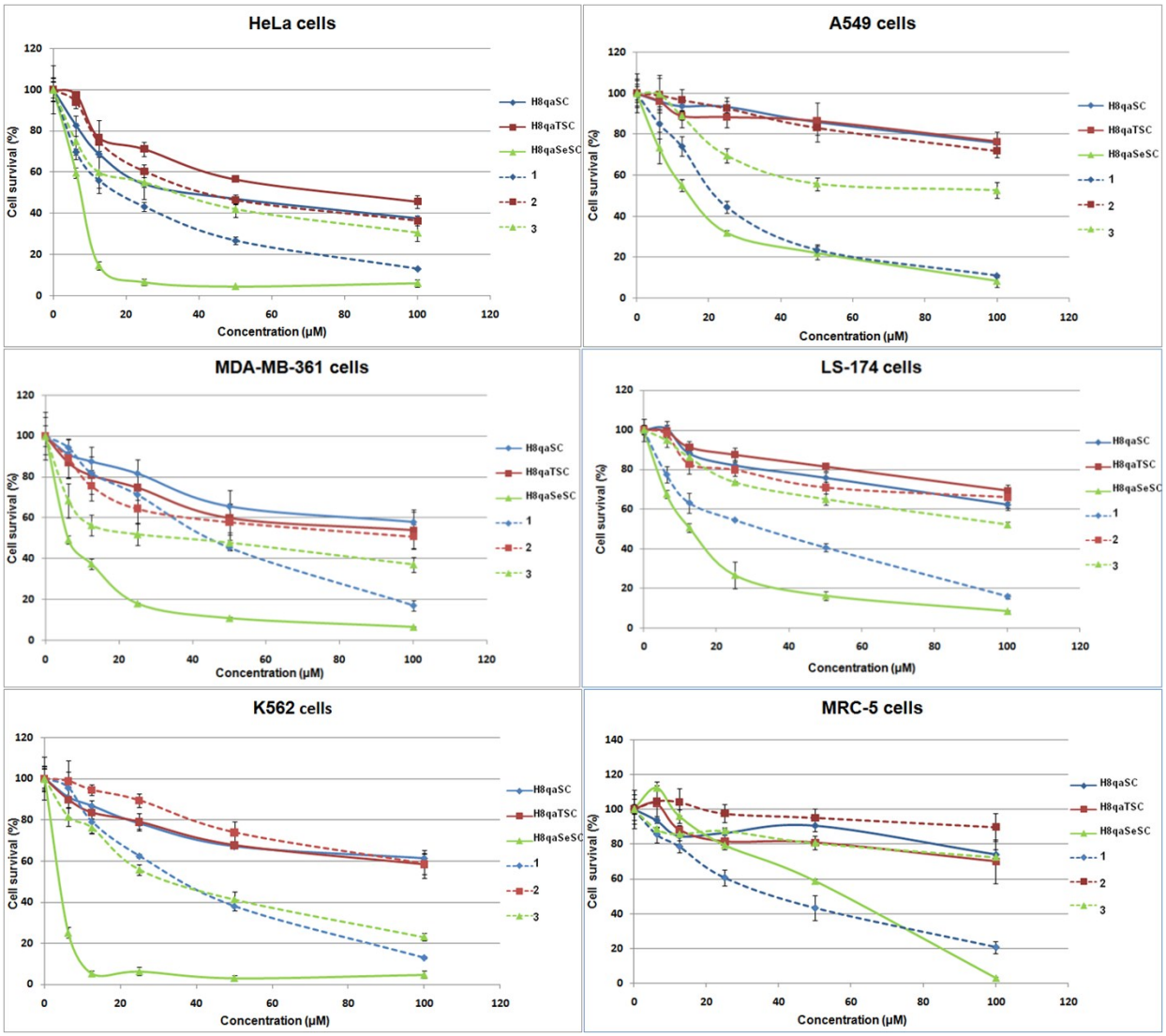

Figure S11. Cell survival diagrams for HeLa, A549, MDA-MB-361, LS-174, K562 and MRC-5 cells (%) after 48 h of continual action of investigated compounds. Data are representative for one out of three separate experiments with standard deviations.

Cell cycle analysis and mechanistic analysis of cell death

Examination of the histograms of HeLa cells (Figure S11a) indicated that the ligands induced a slight increase in the percent of cells in the sub-G1 phase and a decrease in the percent of cells in the G1 phase (being highest after treatment with selenium ligand) after 48 h treatment. The ligand H8qaSeSC induced clear increase in the percent of cells in S and G2 phases. Increase of concentration of the ligands to $1.5\times IC_{50}$ did not have marked influence on cell cycle perturbations after 48 h treatment. Treatment of HeLa cells with **1** for 48 h induced a concentration-dependent great increase in the percent of cells in the sub-G1 phase (cells with fragmented DNA), reaching 48% compared to 4% for control, and a decrease in the percent of cells in G1 and G2 phases of cell cycle (Figure S11a). The complexes **2** and **3** induced an increase in the percent of cells in sub-G1 phase, a decrease in the percent of cells in the G1 phase and a considerable accumulation of cells in the S and G2 phases (the percentage of cells was increased by approximately two-fold compared with control). An increase in the percent of cells in the S phase may indicate that **2** and **3** interfere with DNA replication, probably causing a delay in replication, considering that the cell cycle is not blocked totally in S phase, since the increase of percent of cells in G2 phase was also noticed. Increase of concentration of the complexes to 1.5×IC50 did not have marked influence on the cell cycle, except in the case of complex **1**.

Considering that selenium ligand H8qaSeSC and **1**–**3** induced more aggressive perturbations of cell cycle after 48 h treatment, contrary to milder changes induced by H8qaSC and H8qaTSC, cell cycle perturbations after 24 h treatment with selenium ligand and complexes **1**–**3** and have been further investigated (Figure S11b). Changes of cell cycle of HeLa cells were detected already after 24 h treatment with H8qaSeSC. Changes induced by **1** and **3** spotted after 48 h treatment (a dramatic increase in the percent of cells in sub-G1 phase for **1** and block in S and G2 phases for **3**) are not detected after 24 h, which can indicate their slower entry into the cell or slower activation of cells response. Changes of cell cycle induced by complex **2** were detected already after 24 h treatment but their intensity and mode remained the same as for 48 h treatment.

Considering that among complexes, only complex **1** displayed cytotoxicity on A549 cells, comparable to the activity of CDDP, its effect on cell cycle progression of the A549 cells was examined after continual treatment for 24 and 48 h. Examination of the histograms of A549 cells (Figure S11c) indicated that **1** did not induce any perturbations of the cell cycle after 24 h treatment. Even after prolonged treatment (48 h), perturbations of cell cycle were small, with slight increase of percent of cells in sub-G1 phase.

In general, trend of changes of HeLa cell cycle induced by complexes **2** and **3** (with sulfur and selenium ligands, respectively) were similar to each other, indicating influence on DNA replication, with some potential of DNA fragmentation. The complex **1** with oxygen ligand had a quite different effect, indicating preferential potential of DNA fragmentation.

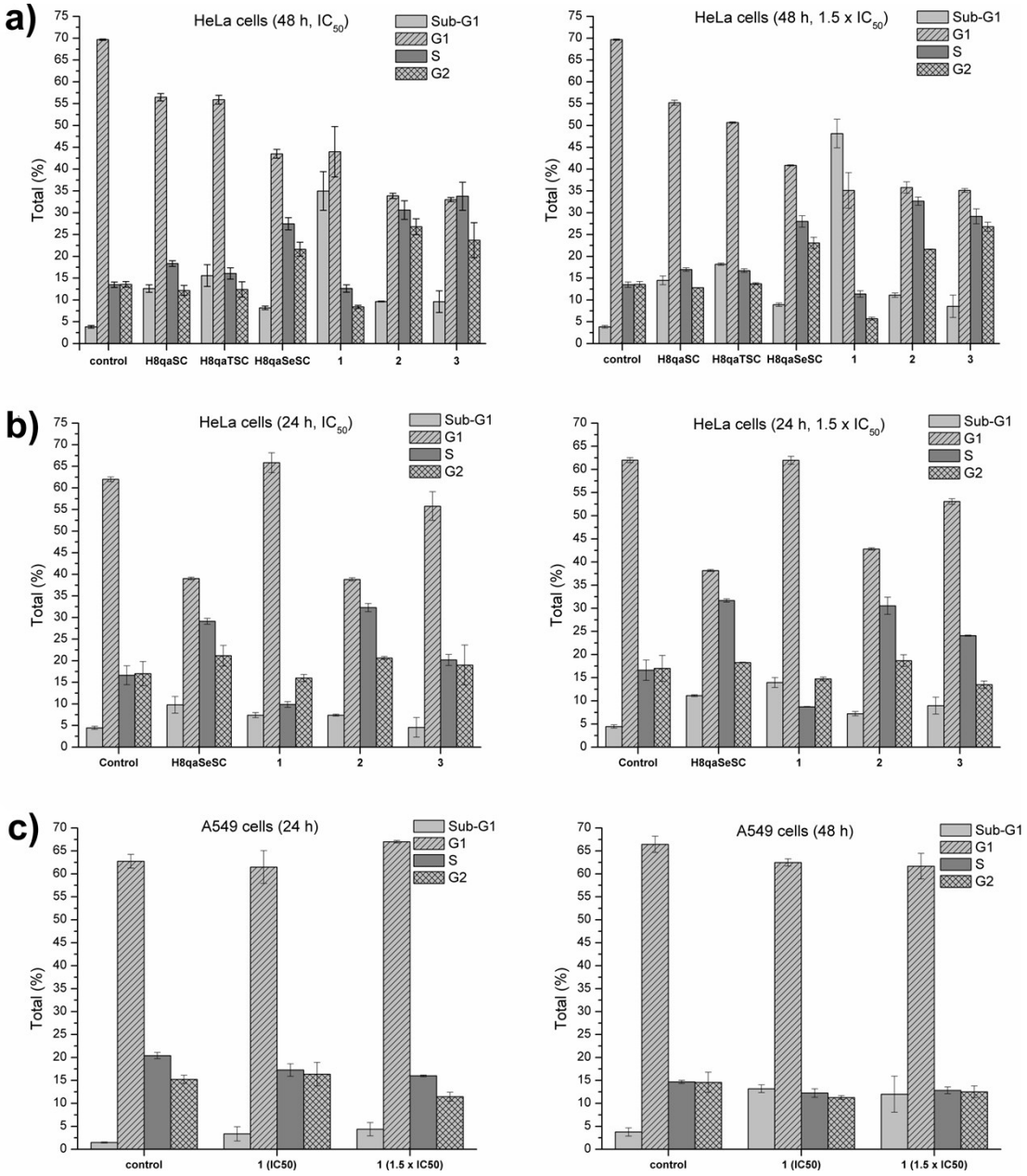

Figure S12. (a) Histograms of 48 h cell cycle distribution of HeLa cells: control and following treatment with the ligands and complexes **1**–**3** (IC_{50} left panel and 1.5 × IC_{50} right panel). (b) Histograms of 24 h cell cycle distribution of HeLa cells: control and following treatment with H8qaSeSC and complexes **1**–**3** (IC_{50} left panel and 1.5 × IC_{50} right panel). (c) Histograms of 24 (left panel) and 48 h (right panel) cell cycle distribution of A549 cells: controls and following treatment with **1** (IC_{50} and 1.5 × IC_{50}). All data represent mean ± SD of three independent experiments.

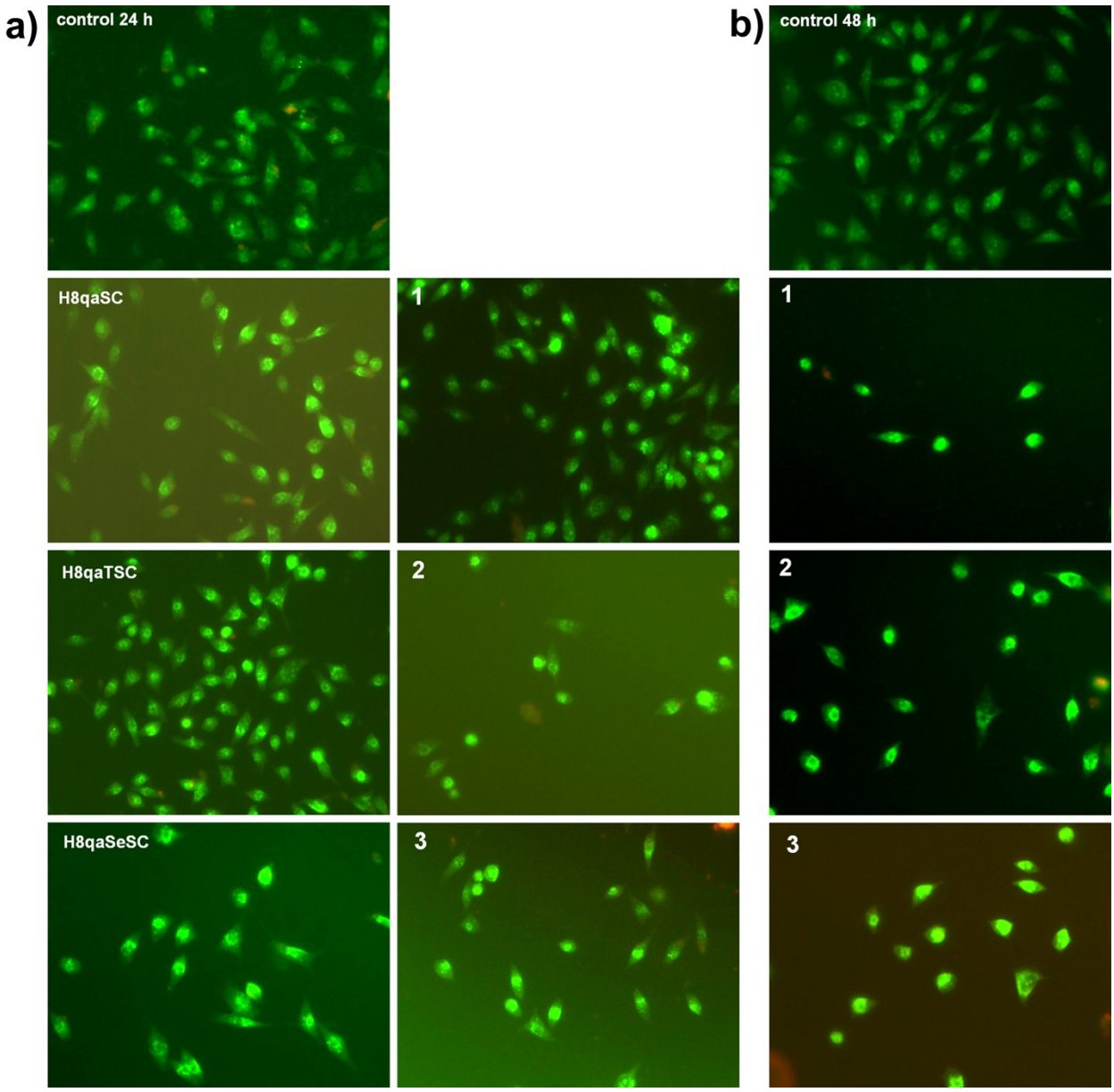

Figure S13. Fluorescent micrographs of double stained HeLa cells with AO and EB: (a) untreated (control) and cells exposed to IC_{50} concentrations of the ligands and complexes **1–3** for 24 h; (b) untreated (control) and cells exposed to IC_{50} concentrations of the complexes **1–3** for 48 h.

The externalization of phosphatidylserine on the outer surface of the plasma membrane is a known hallmark of apoptosis or cell necrosis, depending on cell membrane integrity [S16]. Flow cytometry analysis of double stained treated cells with Annexin-V–FITC (which binds to externalized phosphatidylserine) and PI (membrane-impermeable DNA stain) enables discernment of viable cells (A^-P^-), early apoptotic cells (A^+P^-), late apoptotic cells (A^+P^+) and necrotic cells (A^-P^+). Potential of the ligands and complexes **1**–**3** to induce apoptotic cell death was determined by flow cytometry analysis of Annexin-V–FITC/PI double stained HeLa cells treated for 24 and 48 h (Figure S13).

After 24 h exposure to investigated compounds cell membrane changes through externalization of phosphatidylserine and PI permeability were not observed, except in the case of CDDP (Figure S13). However, after 48 h treatment, the ligands induced increase in the percent of early apoptotic cells from 2.4% in control cells up to 29% (for H8qaSeSC). Selenium ligand had the most similar effect to CDDP. Complex **1** induced increase of percent of cells in early apoptosis (14%) and already dead cells with damaged plasma membranes (A^-P^+, 7%), which indicates that investigated complex has a potential of inducing apoptosis. Complex **2** induced enormous increase of percent of cells in early apoptosis (42%) which indicates that this complex dominantly induces apoptotic cell death, even more than CDDP does. After 48 h treatment with selenium complex **3** the majority of the cells (62%) were with ruptured membrane *i.e.* already dead. However, based solely on these results it is not possible to give precise information which type of cell death was caused by the cytotoxic action of complex **3**. These results highlighted H8qaSeSC ligand, with similar apoptotic potential like CDDP, and complex **2** with even stronger apoptotic potential than CDDP, having in mind that applied concentrations in this test (IC_{50}) were not cytotoxic to normal cells MRC-5.

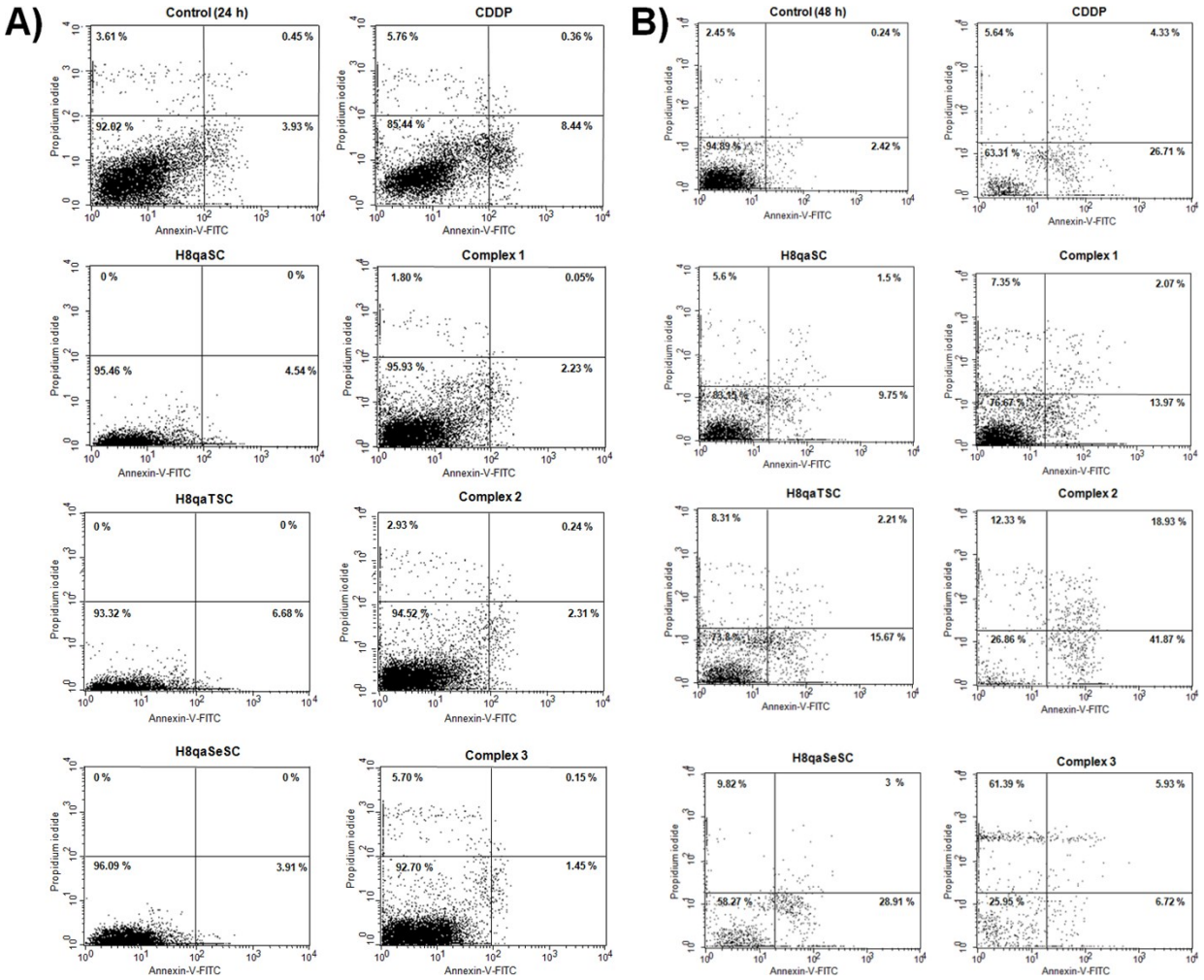

Figure S14. Representative dot plot diagrams obtained by flow cytometry of Annexin-V–FITC/PI double-stained HeLa cells: untreated (control) or treated with the ligands, **1-3** and CDDP with concentration corresponding to IC_{50}, for 24 h (A) and 48 h (B) treatment. A^-PI^- (lower left quadrant) are viable cells, A^+PI^- (lower right quadrant) are early apoptotic cells, A^+PI^+ (upper right quadrant) are late apoptotic cells and A^-PI^+ (upper left quadrant) are necrotic cells.

REFERENCES

[S1] N. Filipović, N. Polović, B. Rašković, S. Misirlić-Denčić, M. Dulović, M. Savić, M. Nikšić, D. Mitić, K. Anđelković, T. Todorović, *Monatsh. Chem*. 145 (2014) 1089–1099. doi: 10.1007/s00706-014-1197-6

[S2] M.D. Revenko, P.N. Bourosh, E.F. Stratulat, I.D. Corja, M. Gdaniec, Yu.A. Simonov, F. Tuna, *Russ. J. Inorg. Chem.* 54 (2009) 530–538. doi:10.1134/S003602360904007X

[S3] M.D. Revenko, P.N. Bourosh, E.F. Stratulat, M. Gdaniec, Ya. Lipkowski, I.D. Korzha, Yu.A. Simonov, *Russ. J. Inorg. Chem*. 55 (2010) 1387–1397. doi:10.1134/S0036023610090093

[S4] N.R. Filipović, S. Bjelogrlić, G. Portalone, S. Pelliccia, R. Silvestri, O. Klisurić, M. Senćanski, D. Stanković, T.R. Todorović, C.D. Muller, *MedChemComm* (2016) in press. doi: 10.1039/C6MD00199H

[S5] Oxford Diffraction CrysAlis Software System; Oxford Diffraction Ltd, 2008.

[S6] L.J. Farrugia, *J. Appl. Crystallogr.* 45 (2012) 849–854. doi:10.1107/S0021889812029111

[S7] M.C. Burla, M. Camalli, B. Carrozzini, G.L. Cascarano, C. Giacovazzo, G. Polidori, R. Spagna, *J. Appl. Crystallogr.* 36 (2003) 1103. doi:10.1107/S0021889803012585

[S8] G.M. Sheldrick, *Acta Crystallogr.* A64 (2008) 112–122. doi:10.1107/S0108767307043930

[S9] A.L. Spek, *J. Appl. Crystallogr.* 36 (2003) 7–13. doi:10.1107/S0021889802022112

[S10] F. Muller, H. Rollag, S.S. Froland, *Clin. Exp. Immunol*. 82 (1990) 10–15.

[S11] R. Supino, Methods in Molecular Biology, in: S. O'Hare, C.K. Atterwill (Eds.), *In Vitro* Toxicity Testing Protocols, Humana Press, New Jersey, 1995, pp. 137–149.

[S12] N. Gligorijević, T. Todorović, S. Radulović, D. Sladić, N. Filipović, D. Gođevac, D. Jeremić, K. Anđelković, *Eur. J. Med. Chem.* 44 (2009) 1623–1629. doi:10.1016/j.ejmech.2008.07.033

[S13] M.G. Ormerod, Analysis of DNA-General Methods, in: M.G. Ormerod (Ed.), Flow Cytometry, a Practical Approach, Oxford University Press, New York, 1994, pp. 119–125.

[S14] M. Milenković, A. Pevec, I. Turel, M. Vujčić, M. Milenković, K. Jovanović, N. Gligorijević, S. Radulović, M. Swart, M. Gruden-Pavlović, K. Adaila, B. Čobeljić, K. Anđelković, *Eur. J. Med. Chem.* 87 (2014) 284–297. doi:10.1016/j.ejmech.2014.06.079

[S15] N.K. Banada, W.C. Satterfield, A. Dunlap, K.S. Steimer, R. Kurrle, T.H. Finkel, *Apoptosis* 1 (1996) 49–62. doi:10.1007/BF00142078

[S16] C. Qian, J.Q. Wang, C.L. Song, L.L. Wang, L.N. Ji, H. Chao, *Metallomics 5* (2013) 844–854. doi:10.1039/C3MT20270D